On the Impact of Redundant Subcarrier Energy Optimization in UW-OFDM

Christian Hofbauer and Mario Huemer, *Senior Member, IEEE,*
Klagenfurt University
Institute of Networked and Embedded Systems
Universitaetsstr. 65-67, 9020 Klagenfurt
chris.hofbauer@uni-klu.ac.at, mario.huemer@uni-klu.ac.at

Johannes B. Huber, *Fellow, IEEE*
University of Erlangen-Nuremberg
Institute for Information Transmission
Cauerstr. 7, D-91058 Erlangen
huber@lnt.de

***Abstract*—Unique word - orthogonal frequency division multiplexing (UW-OFDM) is a novel OFDM concept that uses deterministic sequences, which we call unique words, as guard intervals instead of the conventional cyclic prefixes. Since unique words represent known sequences, they can advantageously be used for sychronization, channel estimation, but also for improving the bit error ratio (BER) behavior of a system. These UWs are created by appropriately loading so-called redundant subcarriers. In this paper, we investigate methods to improve the BER behavior of UW-OFDM by increasing the number of redundant subcarriers (while keeping the length of the UW constant). This gain in the BER performance comes with an increase of the redundancy part and thus with a decrease of the data rate. As such, we present methods to vary the coding rate in UW-OFDM. We present results for the additive white Gaussian noise (AWGN) channel as well as for indoor multipath environments to highlight the advantages of the proposed methods.**

I. Introduction

In mobile communications, multipath propagation is a crucial phenomenon which we have to cope with. Mobile radio channels in indoor or cellular environments can exhibit relatively large time dispersions, i.e. intersymbol interference (ISI). In orthogonal frequency division multiplexing (OFDM) systems, ISI can easily be eliminated by introducing a guard interval between two consecutive OFDM symbols. Furthermore, implementing these guard intervals as cyclic prefixes (CPs) [1] transforms the linear convolution of the transmit signal with the channel impulse response into a cyclic convolution, allowing for a low complexity equalization in the frequency domain. The same can also be achieved by using unique words (UWs) instead of CPs. Nevertheless, there are some fundamental differences between the CP-based and UW-based transmission:

- The UW is part of the discrete Fourier transform (DFT) interval, whereas the CP is not (cf. Fig. 1).
- The CP is random, whereas the UW is a known deterministic sequence, which can advantageously be used for synchronization [2] and channel estimation [3] purposes.
- The implementation of a UW in the time domain introduces correlations in the frequency domain. These correlations can be exploited to improve the bit error ratio (BER) behavior of the system [4].

Christian Hofbauer has been funded by the European Regional Development Fund and the Carinthian Economic Promotion Fund (KWF) under grant 20214/15935/23108.

The UWs are created by appropriately loading so-called redundant subcarriers. By this, correlations along the frequency domain vector of an OFDM symbol are introduced. Investigations in [4] have shown that the energy spent for the redundant subcarriers is critical. In this paper, we extend the results of [4] by increasing the number of redundant subcarriers (while keeping the same length for the UW). By this, the total energy on the redundant subcarriers is reduced and thus the BER performance improved. However, this gain in the BER behavior leads to a decrease of the data rate. As such, the presented ideas can be seen as methods to vary the coding rate in UW-OFDM. In the following, we will refer to this coding rate as "inner coding rate".

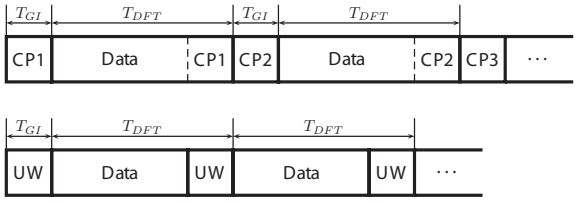

Fig. 1. Transmit data structure using CPs (above) or UWs (below).

The rest of the paper is organized as follows: In section II, we describe our approach of how to introduce unique words in OFDM symbols. Furthermore, we present methods to decrease the energy of the redundant subcarrier symbols by changing the inner coding rate of the system. Section III introduces a linear minimum mean square error (LMMSE) receiver that exploits the correlations introduced by the redundant subcarriers. Section IV evaluates the impact of the energy of the redundant subcarrier symbols on the BER behavior by means of simulations, and section V concludes our work.

Notation Lower-case bold face variables ($\mathbf{a}, \mathbf{b}$,...) indicate vectors, and upper-case bold face variables ($\mathbf{A}, \mathbf{B}$,...) indicate matrices. To distinguish between time and frequency domain variables, we use a tilde to express frequency domain vectors and matrices ($\tilde{\mathbf{a}}, \tilde{\mathbf{A}}$,...), respectively. We further use $\mathbb{C}$ to denote the set of complex numbers, $\mathbf{I}$ to denote the identity matrix, $(\cdot)^T$ to denote transposition, $(\cdot)^H$ to denote conjugate

transposition, $(\cdot)^\dagger$ to denote the Pseudo-Inverse, and $E(\cdot)$ to denote expectation.

II. Unique Word Generation for OFDM

In conventional CP-OFDM, the data vector $\tilde{\mathbf{d}} \in \mathbb{C}^{N_d \times 1}$ is defined in the frequency domain. Typically, zero subcarriers are inserted at the band edges and at the DC subcarrier position, which can formally be described by a matrix operation $\tilde{\mathbf{x}} = \mathbf{B}\tilde{\mathbf{d}}$ with $\tilde{\mathbf{x}} \in \mathbb{C}^{N \times 1}$ and $\mathbf{B} \in \mathbb{C}^{N \times N_d}$. $\mathbf{B}$ consists of zero-rows at the positions of the zero subcarriers, and of appropriate unit row vectors at the positions of data subcarriers. The vector $\tilde{\mathbf{x}}$ denotes the OFDM symbol in frequency domain. The vector of time domain samples $\mathbf{x} \in \mathbb{C}^{N \times 1}$ is calculated via an IDFT (inverse DFT) operation, which can conveniently be formulated in matrix notation by $\mathbf{x} = \mathbf{F}_N^{-1}\tilde{\mathbf{x}}$. Here, $\mathbf{F}_N$ is the N-point-DFT matrix defined by $\mathbf{F}_N = (f_{mn})$ with $f_{mn} = w^{mn}$ for $m = 0, 1, ..., N-1$, $n = 0, 1, ..., N-1$, and with $w = \mathrm{e}^{-j2\pi/N}$.

We now modify this conventional approach by introducing a pre-defined sequence $\mathbf{x}_u$ with $\mathbf{x}_u \in \mathbb{C}^{N_u \times 1}$, which we call unique word, and which shall form the tail of the time domain vector, which we now denote by $\mathbf{x}'$. Hence, $\mathbf{x}'$ consists of two parts and is given by $\mathbf{x}' = \begin{bmatrix}\mathbf{x}_d^T & \mathbf{x}_u^T\end{bmatrix}^T$, where $\mathbf{x}_d \in \mathbb{C}^{(N-N_u)\times 1}$ and $\mathbf{x}_u \in \mathbb{C}^{N_u \times 1}$. The vector $\mathbf{x}_u$ represents the UW of length N_u, and thus only $\mathbf{x}_d$ is random and affected by the data. We use a two step approach [5] to generate the so-defined vector $\mathbf{x}'$:

- In a first step, we will generate a zero UW $\mathbf{x} = \begin{bmatrix}\mathbf{x}_d^T & \mathbf{0}^T\end{bmatrix}^T$, such that $\mathbf{x} = \mathbf{F}_N^{-1}\tilde{\mathbf{x}}$.
- In a second step, we will determine the transmit symbol by $\mathbf{x}' = \mathbf{x} + \begin{bmatrix}\mathbf{0}^T & \mathbf{x}_u^T\end{bmatrix}^T$.

We now describe the first step in detail: As in conventional OFDM, the QAM data symbols and the zero subcarriers are specified in the frequency domain in vector $\tilde{\mathbf{x}}$, but here in addition, the zero word is specified in the time domain as part of the vector $\mathbf{x}$. As a consequence, the linear system of equations $\mathbf{x} = \mathbf{F}_N^{-1}\tilde{\mathbf{x}}$ can only be fulfilled by reducing the number N_d of data subcarriers, and by introducing a set of redundant subcarriers instead. We let the redundant subcarriers form the vector $\tilde{\mathbf{r}} \in \mathbb{C}^{N_r \times 1}$, requiring $N_r \geq N_u$. Additionally, we redefine the dimensions of $\mathbf{B}$ such that $\mathbf{B} \in \mathbb{C}^{N \times (N_d+N_r)}$, further introduce a permutation matrix $\mathbf{P} \in \mathbb{C}^{(N_d+N_r)\times(N_d+N_r)}$, and form an OFDM symbol (containing $N - N_d - N_r$ zero subcarriers) in frequency domain by $\tilde{\mathbf{x}} = \mathbf{BP}\begin{bmatrix}\tilde{\mathbf{d}}^T & \tilde{\mathbf{r}}^T\end{bmatrix}^T$. We will detail the reason for the introduction of the permutation matrix and its specific construction shortly below. Fig. 2 illustrates this approach in a graphical way: The input of the IDFT block is composed of data subcarrier symbols ($\tilde{\mathbf{d}}$), zero subcarriers, and redundant subcarrier symbols ($\tilde{\mathbf{r}}$), which are distributed over the entire non-zero part of vector $\tilde{\mathbf{x}}$ as specified by the permutation matrix $\mathbf{P}$. The output of the IDFT block, which corresponds to the vector $\mathbf{x}$ of time domain samples of an OFDM symbol, is composed of the random part $\mathbf{x}_d$, and the zero UW $\mathbf{0}$.

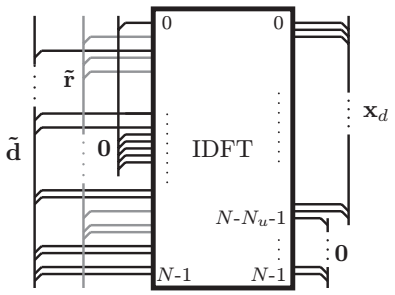

Fig. 2. Time- and frequency-domain view of an OFDM symbol in UW-OFDM.

The relation between the time and the frequency domain representation of an OFDM symbol can now be written as

$$\mathbf{F}_N^{-1}\mathbf{BP}\begin{bmatrix}\tilde{\mathbf{d}}\\ \tilde{\mathbf{r}}\end{bmatrix} = \begin{bmatrix}\mathbf{x}_d\\ \mathbf{0}\end{bmatrix}. \tag{1}$$

With

$$\mathbf{M} = \mathbf{F}_N^{-1}\mathbf{BP} = \begin{bmatrix}\mathbf{M}_{11} & \mathbf{M}_{12}\\ \mathbf{M}_{21} & \mathbf{M}_{22}\end{bmatrix}, \tag{2}$$

where $\mathbf{M}_{ij}$ are appropriately sized sub-matrices, it follows that $\mathbf{M}_{21}\tilde{\mathbf{d}} + \mathbf{M}_{22}\tilde{\mathbf{r}} = \mathbf{0}$. In the following, we will distinguish between two different cases, namely $N_r = N_u$ and $N_r > N_u$.

In case of $N_r = N_u$, the problem to be solved translates to a linear system of equations with N_u equations for N_u unknowns and thus is uniquely solvable. More in detail, $\mathbf{M}_{22}$ becomes a quadratic matrix of dimension $N_u \times N_u$ with a uniquely defined inverse, leading to $\tilde{\mathbf{r}} = -\mathbf{M}_{22}^{-1}\mathbf{M}_{21}\tilde{\mathbf{d}}$. With the matrix $\mathbf{T} = -\mathbf{M}_{22}^{-1}\mathbf{M}_{21} (\mathbf{T} \in \mathbb{C}^{N_r \times N_d})$, the vector of redundant subcarrier symbols can thus be determined by the linear mapping

$$\tilde{\mathbf{r}} = \mathbf{T}\tilde{\mathbf{d}}. \tag{3}$$

It is clear now how to load $\tilde{\mathbf{r}}$ in order to create the desired zero word as UW. However, as we have already mentioned that the energy present on the redundant subcarriers is critical, we additionally wish to minimize this energy. In case of $N_r = N_u$, the choice of the permutation matrix is the only degree of freedom to achieve this. The permutation matrix $\mathbf{P}$ determines the positions of the redundant subcarriers $\tilde{\mathbf{r}}$ within $\tilde{\mathbf{x}}$. Since changing the positions based on the current data $\tilde{\mathbf{d}}$ and therefore during transmission seems impracticable, we thus would like to find a $\mathbf{P}$ such that the energy of $\tilde{\mathbf{r}}$ is minimized over all possible data vectors on average, i.e. minimizing $E\left(\tilde{\mathbf{r}}^H\tilde{\mathbf{r}}\right)$. Assuming i.i.d. zero-mean data QAM symbols with variance σ_d^2 and taking into account (3), this leads to the following optimization problem:

$$\mathbf{P} = \arg\min\{\mathrm{tr}(\mathbf{T}\mathbf{T}^H)\}. \tag{4}$$

It turns out that the right choice of $\mathbf{P}$ is very critical with respect to the resulting energy on $\tilde{\mathbf{r}}$. Experiments show that an approximately equidistant distribution of the redundant subcarriers provides low energy, whereas bundles of them result in extremely high energy values. In section IV, we will

present some optimal distributions for different values of N_r obtained from heuristic optimization methods.

In case of $N_r > N_u$, the problem to be solved translates to an underdetermined linear system of equations and thus provides infinitely many solutions. Besides the choice of the permutation matrix $\mathbf{P}$, we have now an additional degree of freedom to minimize the energy on the redundant subcarriers, leading to the following optimization criterion:

$$\min \|\tilde{\mathbf{r}}\|_2 \text{ s.t. } \mathbf{M}_{21}\tilde{\mathbf{d}} + \mathbf{M}_{22}\tilde{\mathbf{r}} = 0. \tag{5}$$

Here, $\|\cdot\|_2$ denotes the Euclidean norm defined as $\|\tilde{\mathbf{r}}\|_2 = \sqrt{\tilde{\mathbf{r}}^H\tilde{\mathbf{r}}}$. Note that in contrast to (4), we aim at finding the optimum for each individual transmit symbol instead of just finding the optimum on average. This means that we take into account the actual data subcarrier symbols $\tilde{\mathbf{d}}$ instead of their statistical properties. Eq. (5) is met with optimality by the Pseudo-Inverse defined as $\mathbf{M}_{22}^{\dagger} = \left(\mathbf{M}_{22}^H\mathbf{M}_{22}\right)^{-1}\mathbf{M}_{22}^H$ ($\mathbf{M}_{22}^{\dagger} \in \mathbb{C}^{N_r \times N_u}$), leading to $\tilde{\mathbf{r}} = -\mathbf{M}_{22}^{\dagger}\mathbf{M}_{21}\tilde{\mathbf{d}}$. With $\mathbf{T} = -\mathbf{M}_{22}^{\dagger}\mathbf{M}_{21} (\mathbf{T} \in \mathbb{C}^{N_r \times N_d})$ we arrive at the linear mapping as in (3).

For both cases, i.e. independent of $N_r = N_u$ or $N_r > N_u$, we can now use the notation $\tilde{\mathbf{s}}$ with

$$\tilde{\mathbf{s}} = \mathbf{P}\begin{bmatrix}\tilde{\mathbf{d}}\\ \tilde{\mathbf{r}}\end{bmatrix} = \mathbf{P}\begin{bmatrix}\mathbf{I}\\ \mathbf{T}\end{bmatrix}\tilde{\mathbf{d}} = \mathbf{G}\tilde{\mathbf{d}}, \tag{6}$$

($\tilde{\mathbf{s}} \in \mathbb{C}^{(N_d+N_r)\times 1}, \mathbf{G} \in \mathbb{C}^{(N_d+N_r)\times N_d}$) for the non-zero part of $\tilde{\mathbf{x}}$, such that $\tilde{\mathbf{x}} = \mathbf{B}\tilde{\mathbf{s}}$. Finally, the transmit symbol $\mathbf{x}'$ is generated by adding the unique word like described earlier. The frequency domain representation $\tilde{\mathbf{x}}'_u \in \mathbb{C}^{N\times 1}$ of the UW is defined by $\tilde{\mathbf{x}}'_u = \mathbf{F}_N\begin{bmatrix}\mathbf{0}^T & \mathbf{x}_u^T\end{bmatrix}^T$. Note that $\mathbf{x}'$ can also be written as $\mathbf{x}' = \mathbf{F}_N^{-1}(\tilde{\mathbf{x}}'_u + \tilde{\mathbf{x}}) = \mathbf{F}_N^{-1}(\tilde{\mathbf{x}}'_u + \mathbf{B}\tilde{\mathbf{s}})$. The mean energy $E_{\mathbf{x}'}$ of the transmit symbol $\mathbf{x}'$ can be shown to be

$$E_{\mathbf{x}'} = \frac{1}{N}(\underbrace{N_d\sigma_d^2}_{E_{\tilde{\mathbf{d}}}} + \underbrace{\sigma_d^2\mathrm{tr}\left(\mathbf{T}\mathbf{T}^H\right)}_{E_{\tilde{\mathbf{r}}}}) + \underbrace{\mathbf{x}_u^H\mathbf{x}_u}_{E_{\mathbf{x}_u}}. \tag{7}$$

$\frac{E_{\tilde{\mathbf{d}}}}{N}$ and $\frac{E_{\tilde{\mathbf{r}}}}{N}$ describe the contributions of the data and the redundant subcarrier symbols to the total mean symbol energy before the addition of the UW, respectively, and $E_{\mathbf{x}_u}$ describes the contribution of the UW. We will refer back to this equation more in detail in section IV.

III. OFDM RECEIVER

Let $\mathbf{x}'$ be the transmit symbol, then after the transmission over a multipath channel and after the common DFT operation (preferably implemented as FFT (fast Fourier transform)), the non-zero part $\tilde{\mathbf{y}} \in \mathbb{C}^{(N_d+N_r)\times 1}$ of a received OFDM frequency domain symbol can be modeled as $\tilde{\mathbf{y}} = \mathbf{B}^T\mathbf{F}_N\mathbf{H}\mathbf{F}_N^{-1}(\tilde{\mathbf{x}}'_u + \mathbf{B}\tilde{\mathbf{s}}) + \mathbf{B}^T\mathbf{F}_N\mathbf{n}$, where $\mathbf{H}$ denotes a cyclic convolution matrix with $\mathbf{H} \in \mathbb{C}^{N\times N}$, and $\mathbf{n} \in \mathbb{C}^{N\times 1}$ represents a noise vector with the covariance matrix $\sigma_n^2\mathbf{I}$. The multiplication with $\mathbf{B}^T$ excludes the zero subcarriers from further operation. The matrix $\mathbf{F}_N\mathbf{H}\mathbf{F}_N^{-1}$ is diagonal and contains the sampled channel frequency response on its main diagonal. $\tilde{\mathbf{H}} = \mathbf{B}^T\mathbf{F}_N\mathbf{H}\mathbf{F}_N^{-1}\mathbf{B}$ with $\tilde{\mathbf{H}} \in \mathbb{C}^{(N_d+N_r)\times(N_d+N_r)}$ is a down-sized version of $\mathbf{F}_N\mathbf{H}\mathbf{F}_N^{-1}$ excluding the entries corresponding to the zero subcarriers. The received symbol can therefore also be formulated as

$$\tilde{\mathbf{y}} = \tilde{\mathbf{H}}(\mathbf{B}^T\tilde{\mathbf{x}}'_u + \tilde{\mathbf{s}}) + \mathbf{B}^T\mathbf{F}_N\mathbf{n}. \tag{8}$$

One can show that the LMMSE [6] receiver can be written as

$$\widehat{\tilde{\mathbf{d}}} = \tilde{\mathbf{W}}\tilde{\mathbf{H}}^{-1}\left(\tilde{\mathbf{y}} - \tilde{\mathbf{H}}\mathbf{B}^T\tilde{\mathbf{x}}'_u\right), \tag{9}$$

whereas the Wiener smoothing matrix $\tilde{\mathbf{W}}$ is given by

$$\tilde{\mathbf{W}} = \mathbf{G}^H\left(\mathbf{G}\mathbf{G}^H + \frac{N\sigma_n^2}{\sigma_d^2}\left(\tilde{\mathbf{H}}^H\tilde{\mathbf{H}}\right)^{-1}\right)^{-1}. \tag{10}$$

Note that the error $\tilde{\mathbf{e}} = \tilde{\mathbf{d}} - \widehat{\tilde{\mathbf{d}}}$ has zero mean, and its covariance matrix is given by [6] $\mathbf{C}_{\tilde{e}\tilde{e}} = \sigma_d^2\left(\mathbf{I} - \tilde{\mathbf{W}}\mathbf{G}\right)$, which can be further utilized when channel coding is applied. Furthermore, we notice from (9) that we first subtract $\tilde{\mathbf{H}}\mathbf{B}^T\tilde{\mathbf{x}}'_u$ from $\tilde{\mathbf{y}}$ before applying equalization. As such, the specific choice of the UW does not influence the performance of the LMMSE receiver and can thus be chosen independently from that.

IV. PERFORMANCE

This section will demonstrate how the inner coding rate and thus the energy present on the redundant subcarriers influences the performance of the UW-OFDM system in terms of the BER behavior. We will present results for the additive white Gaussian noise (AWGN) case and additionally for two dedicated multipath channel snapshots. Fig. 3 shows the block diagram of the simulated UW-OFDM system. Starting with channel coding, interleaving and mapping, the redundant subcarriers are loaded like indicated in (3). The OFDM symbol in the frequency domain is created by appropriately assembling $\tilde{\mathbf{d}}$, $\tilde{\mathbf{r}}$ and a set of zero subcarriers. Afterwards, an inverse fast Fourier transform (IFFT) is applied, and finally the UW is added in the time domain. At the receiver, we apply a FFT operation followed by a zero forcing (ZF) equalization. Next, the frequency domain representation of the UW is subtracted and a Wiener smoothing operation is applied. Finally, demapping, deinterleaving and decoding are performed. For the decoding step, we use a soft decision Viterbi approach with the main diagonal of the matrix $\mathbf{C}_{\tilde{e}\tilde{e}}$ as an additional input specifying the noise variances along the subcarriers after equalization and Wiener filtering.

We compare our novel UW-OFDM approach with the classical CP-OFDM concept. The IEEE 802.11a WLAN standard [7] serves as reference system. We apply the same parameters for UW-OFDM as in [7] wherever possible: $N = 64$, sampling frequency $f_s = 20$MHz, DFT period $T_{DFT} = 3.2\mu$s, guard duration $T_{GI} = 800$ns, and twelve zero subcarriers at the positions {0, 27, 28,...,37}. Instead of $N_d = 48$ data subcarriers and $N_p = 4$ pilots, we use N_d data subcarriers and N_r redundant subcarriers, whereas $28 \leq N_d \leq 36$ and $16 \leq N_r \leq 24$, depending on the specific configuration. The data symbols are drawn from a QPSK alphabet with variance $\sigma_d^2 = 1$, leading to a total mean energy of the data subcarrier symbols of $\frac{E_{\tilde{\mathbf{d}}}}{N} = \frac{N_d}{64}$. According to the guard duration, the

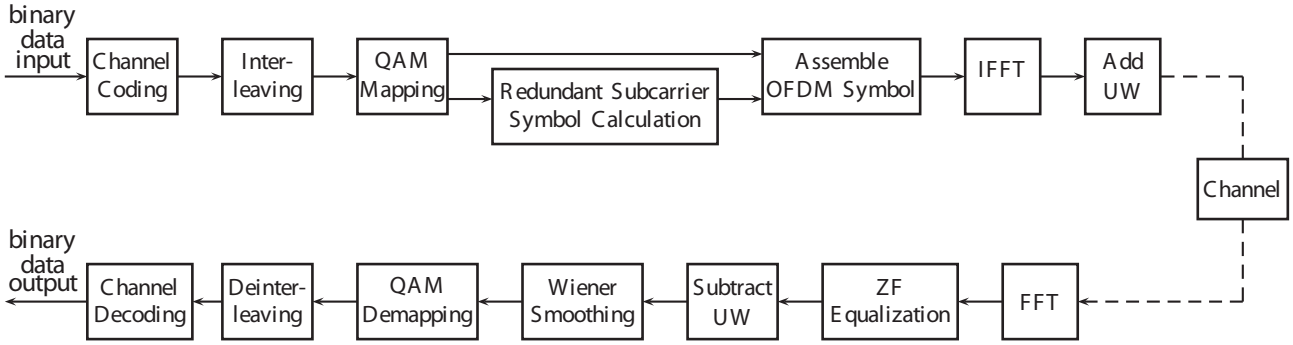

Fig. 3. Block diagram for simulation analysis.

N_r	Index set
16	2,6,10,14,17,21,24,26,38,40,43,47,50,55,58,62
20	1,4,7,10,13,15,18,21,24,26,38,40,43,46,48,51,54,57,59,62
24	2,4,6,9,11,13,16,18,20,22,24,26,38,40,42,44,46,48, 51,54,56,58,60,63

TABLE I
INDICES OF REDUNDANT SUBCARRIERS

	IEEE 802.11a	UW-OFDM		
N_d	48	36	32	28
N_r (N_p)	4	16	20	24
B [MHz]	16.60	16.10	16.20	16.22
η	0.723	0.699	0.617	0.540
η_{rel}	1.000	0.967	0.854	0.746
$E_{\tilde{\mathbf{r}}}$		36.57	24.91	18.41
E_b	0.01058	0.01706	0.01506	0.01483
AWGN loss [dB]	0.0000	2.0754	1.5320	1.2254

TABLE II
PERFORMANCE IEEE 802.11A VS. UW-OFDM

UW has a length of $N_u = 16$. In our approach, this UW shall take over the synchronization tasks which are normally performed with the help of the 4 pilot subcarriers. However, since in this paper, we only focus on the BER behavior of UW-OFDM, and since the performance of the proposed receiver is independent of the UW (see (9)), only the energy $E_{\mathbf{x}_u}$ of the UW but not the specific design is of interest in this case. Due to reasons of fair comparison, the energy $E_{\mathbf{x}_u}$ of the UW related to the total energy of a transmit symbol is set to $\frac{E_{\mathbf{x}_u}}{E_{\mathbf{x}'}} = \frac{4}{52}$, which exactly corresponds to the total energy of the 4 pilots related to the total energy $E_{\mathbf{x},CP}$ of a transmit symbol in the IEEE standard. According to (7), we can thus write $E_{\mathbf{x}'} = \frac{E_{\tilde{\mathbf{d}}}}{64} + \frac{E_{\tilde{\mathbf{r}}}}{64} + \frac{4}{52}E_{\mathbf{x}'}$ and after some reformulations arrive at $E_{\mathbf{x}_u} = \left(\frac{N_d}{64} + \frac{E_{\tilde{\mathbf{r}}}}{64}\right)\frac{52}{48}\frac{4}{52}$. Since we use QPSK mapping (2 bits per symbol), the mean energy per transmit bit is calculated as $E_b = \frac{E_{\mathbf{x}'}}{2N_d}\frac{T_{OFDM}}{T_{DFT}}$. In conventional CP-OFDM like in the IEEE 802.11a standard, the total length of an OFDM symbol T_{OFDM} is given by $T_{GI} + T_{DFT}$. Note that in our approach, the guard interval is already part of the DFT period and thus $T_{OFDM} = T_{DFT}$.

Table I illustrates the subcarrier sets for various numbers of redundant subcarriers which have been used for evaluating the performance of the different UW-OFDM system configurations. These sets have been found by heuristic optimization methods subject to (4). As already mentioned earlier, the optimal sets with respect to achieving low energy on the redundant subcarriers turn out to follow a nearly equidistant distribution. Table II compares our UW-OFDM approach with the IEEE 802.11a system. We notice that our UW-OFDM approach needs about 0.4-0.5MHz less bandwidth B for transmission than the IEEE 802.11a system. These results have been obtained by simulations and measurements of the normalized power spectral density of the transmit bursts at -10dB down from the maximum of the flat region of the spectrum. The third row presents the bandwidth efficiency of the systems measured in megasymbols per seconds per MHz [(Ms/s)/MHz] and is given by $\eta = (N_d/T_{OFDM})/B$. The fourth row shows the bandwidth efficiency of the UW-OFDM systems related to the IEEE 802.11a approach (η_{rel}). We notice that in case of $N_r = 16$, our UW-OFDM approach shows almost the same bandwidth efficiency as the conventional CP-OFDM approach. Increasing now N_r leads of course to less bandwidth efficiency on one hand, but decreases the mean energy $\frac{E_{\tilde{\mathbf{r}}}}{N}$ of the redundant subcarrier symbols and hence the mean energy per transmit bit E_b on the other hand. The AWGN loss is calculated as $10\log_{10}\left(\frac{E_{b,UW}}{E_{b,CP}}\right)$, whereas $E_{b,CP} = 0.01058$ determines the mean energy per bit for the IEEE 802.11a system and $E_{b,UW}$ that of the specific UW-OFDM system. It specifies the loss of UW-OFDM compared to IEEE 802.11a when just a simple zero forcing equalizer (without additional Wiener smoothing) is applied. As such, decreasing E_b for UW-OFDM will decrease this loss. Fig. 4 confirms this effect by means of simulations. At a BER of 10^{-6}, the UW-OFDM without smoothing loses around 2.05dB against the IEEE 802.11a standard in case of $N_r = 16$, 1.55dB for $N_r = 20$ and 1.3dB for $N_r = 24$, respectively. These results coincide with that of table II up to negligible simulation inaccuracies. However, the Wiener smoother exploits the correlations between the subcarriers of an OFDM symbol and improves the performance of the UW-OFDM system in the AWGN channel by around 1.5dB for all investigated modes, leading to a residual performance loss compared to the IEEE

802.11a standard of only 0.55dB for $N_r = 16$ and 0.05dB for $N_r = 20$, respectively. In case of $N_r = 24$, the UW-OFDM system even outperforms the IEEE 802.11a system by 0.2dB. We will show in the following that in case of frequency selective environments (at least for the selected scenarios), the UW-OFDM system always outperforms the IEEE 802.11a system regardless of N_r.

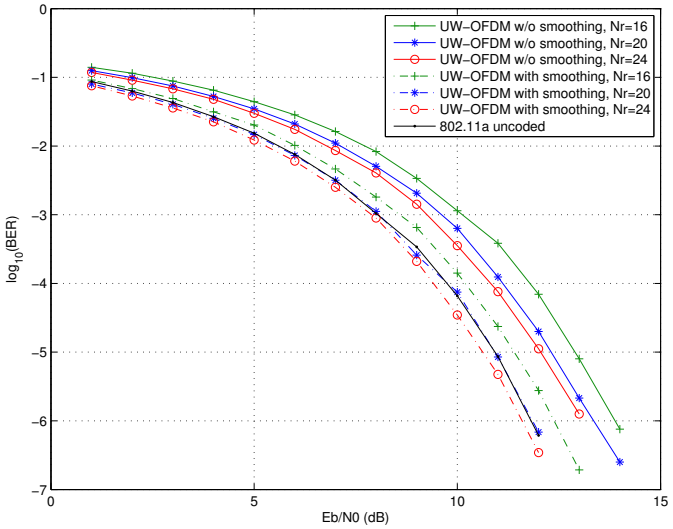

Fig. 4. BER comparison between the novel UW-OFDM approach and the IEEE 802.11a standard in the AWGN channel.

The multipath channel has been modeled as a tapped delay line, each tap with uniformly distributed phase and Rayleigh distributed magnitude, and with power decaying exponentially. A detailed description of the model can be found in [3]. Fig. 5 shows two typical channel snapshots with a channel delay spread of 100ns drawn from this model which we have used to evaluate the performance. These channel snapshots represent typical indoor office environments.

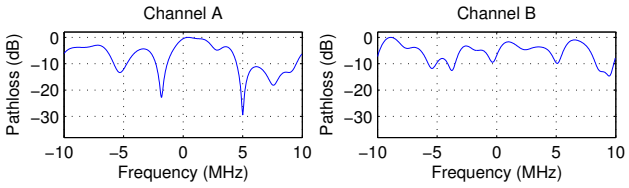

Fig. 5. Frequency responses of the used indoor multipath channel snapshots (equivalent complex baseband presentation as usual).

Fig. 6 shows the BER behavior of the UW-OFDM systems in comparison to the IEEE 802.11a system for channel A in Fig. 5. We simulated the BER behavior with and without additional outer code. The outer code features the coding rates $r = 3/4$ and $r = 1/2$. Both systems use the same convolutional encoder with rate 1/2, constraint length 7 and the generator polynomial (133,171). The code rate $r = 3/4$ is achieved by puncturing as described in [7]. We notice that the higher the (outer) coding rate, the higher the gain achieved by the UW-OFDM approach. In case of $r = 1$, i.e. no outer code, the performance gain is tremendous. For $r = 3/4$, UW-OFDM outperforms IEEE 802.11a by 0.9dB for $N_r = 16$, 2.05dB for $N_r = 20$ and even 3.0dB for $N_r = 24$. In case of $r = 1/2$, we still achieve gains of 0.6dB, 1.0dB and 1.0dB for $N_r = 16, 20$ and 24, respectively. We clearly notice that increasing the redundancy part, i.e. increasing N_r, leads to a gain in the BER on one hand, but also leads to a decrease of the data rate on the other hand. As such, varying N_r has the effect of varying the (inner) coding rate of the system. Fig. 7 shows the results for channel B of Fig. 5. Even though the gains have reduced, we notice similar tendencies. We gain 0.9dB, 1.25dB and 1.75dB in case of $r = 1$ for $N_r = 16, 20, 24$. For $r = 3/4$, we gain 0.7dB, 0.8dB and 1.3dB, and in case of $r = 1/2$ 0.3dB, 0.8dB and 1.1dB, respectively.

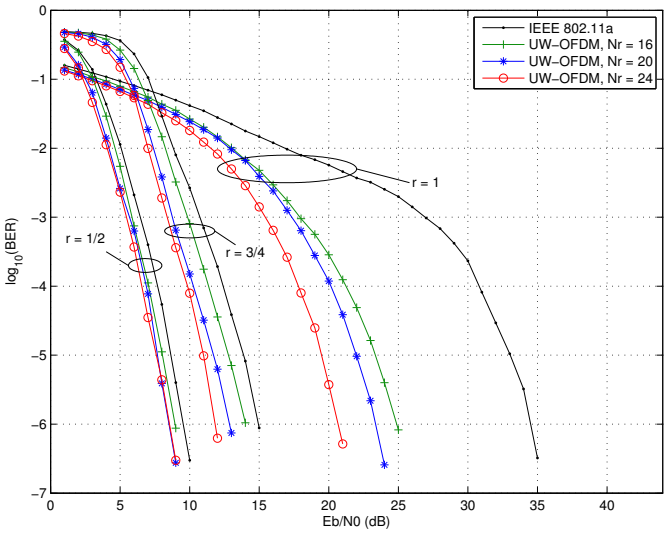

Fig. 6. BER comparison between the novel UW-OFDM approach and the IEEE 802.11a standard for channel A of Fig. 5.

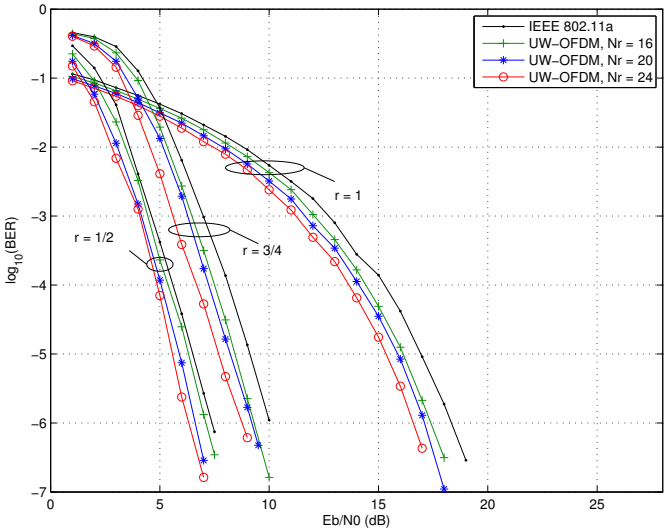

Fig. 7. BER comparison between the novel UW-OFDM approach and the IEEE 802.11a standard for channel B of Fig. 5.

These simulation results have provided some fundamental insights which can be summarized as follows:

- In the AWGN channel and without Wiener smoothing, the IEEE 802.11a system always outerperforms the UW-OFDM approach.
- An increase of the number N_r of redundant subcarriers and thus a decrease of $E_{\tilde{\mathbf{r}}}$ enhances the BER behavior of an UW-OFDM system. This effect can be interpreted as changing the inner coding rate of the system.
- The Wiener smoothing filter additionally improves the BER behavior. Dependent on N_r, the UW-OFDM system may even outperform the IEEE 802.11a system.
- For the investigated frequency-selective scenarios, the UW-OFDM approach always outperforms the IEEE 802.11a system. The specific gain in performance depends on the outer coding rate r, but also on the inner coding rate determined by the number N_r of redundant subcarriers.

V. Conclusion

In this work we demonstrated the relationship between the energy spent for the redundant subcarrier symbols in the frequency domain necessary to create the desired unique word in the time domain, and the BER behavior of such an UW-OFDM system. We showed that by increasing the number of redundant subcarrier symbols, which can be interpreted as changing the inner coding rate of the UW-OFDM system, and by choosing an appropriate distribution of them in the spectrum, the total energy of the redundant subcarrier symbols can be decreased and thus the BER behavior significantly improved. These results have been confirmed for the AWGN case as well as for typical frequency-selective indoor scenarios.

References

[1] R. van Nee, R. Prasad, *OFDM for Wireless Multimedia Communications*, Artech House Publishers, Boston, 2000.

[2] M. Huemer, H. Witschnig, J. Hausner, "Unique Word Based Phase Tracking Algorithms for SC/FDE Systems", In the *Proceedings of the IEEE International Conference on Global Communications (GLOBECOM' 2003)*, San Francisco, USA, 5 pages, December 2003.

[3] H. Witschnig, Frequency Domain Equalization for Broadband Wireless Communication - With Special Reference to Single Carrier Transmission Based on Known Pilot Sequences, Dissertation, University of Linz, 2003.

[4] M. Huemer, C. Hofbauer, J.B. Huber, "The Potential of Unique Words in OFDM", in the *Proceedings of the 15th International OFDM Workshop (InOWo' 10)*, Hamburg, Germany, pp. 140-144 September 2010.

[5] A. Onic, M. Huemer, "Direct versus Two-Step Approach for Unique Word Generation in UW-OFDM", in the *Proceedings of the 15th International OFDM-Workshop 2010 (InOWo' 10)*, Hamburg, Germany, pp.145-149, September 2010.

[6] S. Kay, *Fundamentals of Statistical Signal Processing: Estimation Theory*, Prentice Hall, Rhode Island 1993.

[7] IEEE Std 802.11a-1999, Part 11: Wireless LAN Medium Access Control (MAC) and Physical Layer (PHY) specifications: High-Speed Physical Layer in the 5 GHz Band, 1999.